# Numerical predictions of flow field in closed and opened Taylor-Couette cavities

*Raphaël Guillerm\*, Riccardo Da Soghe\*\*, Cosimo Bianchini\*\*, Sébastien Poncet†\* and Stéphane Viazzo\**

*\*Laboratoire M2P2, UMR 6181 CNRS – Aix-Marseille Université*

*Technopôle Château-Gombert, 38 rue F. Joliot-Curie, 13451 Marseille, France*

*†corresponding author: [poncet@l3m.univ-mrs.fr](poncet@l3m.univ-mrs.fr), Tel. +33(0)491118523, Fax: +33(04)91118502*

*\*\*Energy Engineering Department S. Stecco, University of Florence*

*50139 via S. Marta 3, Florence, Italy*

## Abstract

The accurate prediction of fluid flow within rotating systems has a primary role for the reliability and performance of gas turbine engine. The selection of a suitable model to account for the effects of turbulence on such complex flows remains an open issue in the literature. This paper reports a numerical benchmark of RANS, DES and LES approaches available within the commercial CFD solvers Star CCM+ and CFX together with results obtained by means of in-house developed or open-source available research codes exploiting an innovative Reynolds Stress Model closure, a direct numerical simulation and additional RANS and LES models. The predictions are compared to experimental data available in the literature for two test cases. Test case 1 corresponds to a closed Taylor-Couette cavity with endcap rings, considered experimentally by Burin *et al.* [1]. Test case 2 corresponds to a Taylor-Couette system with an axial Poiseuille flow studied experimentally by Escudier and Gouldson [2]. The results are compared and discussed in details for both the mean and turbulent fields. Most of the approaches predict quite well the trends apart from the SST models, which provide relatively poor agreement with the experiments. Even though no approach appears to be fully satisfactory, the innovative RSM closure offers the best overall agreement in both closed and opened Taylor-Couette cavities.

## 1. Introduction

The present investigation is concerned with the numerical modeling of fluid flow in closed and opened Taylor–Couette systems. The turbulent flow is confined between two coaxial cylinders, with an inner rotating cylinder and an outer stationary one. An axial throughflow of fluid may be superimposed or not. This kind of Taylor–Couette flows with or without an axial Poiseuille flow is of great importance, since they found many applications in process engineering (dynamic membrane filtration, rheology, UV disinfection, chemical mixing devices), in geophysics and astrophysics (mantle convection, accretion disk) and most of all in turbomachineries for bearings, asynchronous motor with axial ventilation, rotating heat exchangers, gas turbine engines and the drilling of oil wells among others.

For example, the Taylor–Couette system with an axial Poiseuille flow considered by Escudier and Gouldson [2] is a simple representation of the gap between the rotating and the stationary parts of an electrical motor. In such a rotating machinery, a better knowledge of the fluid flow is required to better predict the heat transfer distribution and thus to optimize the performances of the device. An uncertainty of 5% on the heat fluxes along the walls is indeed responsible for 60% of the non-scheduled stops. Up to now, only very few works have been dedicated to real industrial flows, which imply very high rotation rates (around $10^5$ rpm) and narrow gap cavity ($\approx$ 1 mm). The difficulty to perform accurate measurements in such clearances and especially in the thin boundary layers along the cylinders is obvious and has slowed down the development of specific turbulence models. Until relatively recently, the turbulent flow regime has been treated, in computations but also in experiments, as though the flow pattern within the cavity were axisymmetric. Treating the turbulent flow as statistically stationary implicitly assumed that the coherent structures present in the transitional modes disappeared or that their effect when averaged out was accounted for in the model without explicit treatment. Owen [3] first suggested that, sometimes, the flow within such cavity might not be steady. In the case of rotating disk systems with throughflow, the RANS model he used failed to converge for a certain range of parameters and he speculated that some form of organized large-scale structure may

have been present in the flow. These 3D patterns might be responsible for some discrepancies between experiments and axisymmetric computations.

The presence of 3D structures is not the only complexity in such flows. High rotation rates, superimposed throughflow, wall effects, three-dimensional boundary layers, the coexistence of laminar, transitional and turbulent regions… are other challenges for numerical approaches. Thus, three-dimensional calculations may be required in some specific configurations. But due to their highly expensive computational cost, the selection of a suitable turbulence model for the study of rotating cavity flows is still pertinent and remains an open issue in the literature. The aim of the present work is then to perform a numerical benchmarking of different RANS, DES and LES models (in-house developed or available within commercial codes) in two different geometries: the first one considered previously by Burin $et$ $al.$ [1] is a low aspect ratio enclosed cavity with endcap rings and the second one is an opened cavity with an axial Poiseuille flow studied by Escudier and Gouldson [2]. In both cases, the approach, which offers the best trade-off between accuracy and calculation cost, will be isolated.

Enclosed Taylor-Couette systems have been widely considered since one of the pioneering work by Wendt [4] because they offer an academic and relatively simple geometry to investigate the influence of rotation on turbulence for fundamental purpose or astrophysics applications. Recently, Burin $et$ $al.$ [1] reported velocity fluctuations and the fluctuation-driven radial transport of angular momentum in a short Taylor-Couette system of low radius ratio: $\Gamma = H / [2 (R_2 – R_1)] = 1.06$ and $\eta = R_1 / R_2 = 0.35$, where $R_1$ and $R_2$ are the radii of the inner and outer cylinders respectively and $H$ is the cavity height. Fluctuation levels and the mean specific angular momentum were found to be roughly constant over radius, in accordance with previous studies featuring narrower gaps. They provided useful velocity measurements for both the mean and turbulent fields and confirmed some scalings established in similar flows for torque and angular momentum transport. Bazilevs and Akkerman [5] presented an application of the residual-based variational multiscale turbulence modeling methodology to the computation of turbulent Taylor–Couette flow at high Reynolds number. Its formulation globally conserves angular momentum, a feature that is felt to be important for flows dominated by rotation, and that is not shared by standard stabilized formulations of fluid flow. We can cite also the DNS results of Dong [6] for turbulent Taylor-Couette flows between counter-rotating cylinders.

The effect of an axial throughflow in a Taylor–Couette system, where only the inner cylinder is rotating, has been considered experimentally by Kaye and Elgar [7] in the isothermal case. Their results showed in particular the existence of four flow regimes depending on the Reynolds number based on the incoming flow velocity and the radial gap between the cylinders and on the Taylor number: laminar and turbulent flows, with or without Taylor vortices. Escudier and Gouldson [2] performed velocity measurements by Laser Doppler Anemometry (LDA) in a cavity characterized by $\Gamma = 116$ and $\eta = 0.506$ for various flow conditions (rotation rate $\Omega$ and flow rate $Q$) and different fluids including Newtonian and shear-thinning fluids. For the Newtonian fluid in the turbulent regime, the radial distribution of the axial velocity and the pressure drop are similar to the ones observed in pipe flows. The radial distribution of the tangential velocity reveals a flow structure divided into three regions: two very thin boundary layers, one on each cylinder, separated by a central core in near solid body rotation. The main effect of the superimposed axial throughflow is to reduce the tangential velocity in the core region. Nouri and Whitelaw [8] measured the three mean velocity components and the associated Reynolds stress tensor of the flow subjected to an axial superimposed throughflow in a concentric annulus ($\eta = 0.5$) with or without rotation of the inner cylinder. Compared to the non-rotating case (for a given flow rate coefficient $C_w = Q/ (v R_2) = 42\ 306$), the rotation of the inner cylinder at $\Omega = 300\ rpm$ (rotational Reynolds number $Re = \Omega R_1 (R_2 – R_1)/v = 1616.6$) does not affect the drag coefficient and the radial distribution of the mean axial velocity in the turbulent regime. It slightly enhances turbulence intensities especially close to the walls. For $C_w = 125\ 039$, there is absolutely no effect of the rotation of the inner shaft on both the mean axial flow and turbulence intensities. In a subsequent paper, Nouri and Whitelaw [9] extended their work to the case of eccentric cylinder arrangements and proposed a review of previous works on Taylor–Couette flows including Newtonian and non-Newtonian fluids and rotating and non-rotating flows. Naser [10] compared the predictions of a k–ε model with the experimental data of Escudier and Gouldson [2] for the same flow conditions. For a turbulent Newtonian flow, the model showed large discrepancies for the mean velocity components. The profiles depend strongly on the axial position, which is not observed in the experiments [2]. Naser [10] attributed these deviations to the fact that the eddy viscosity concept, on which the model is developed, is incompatible with the simulated flow conditions. It can be attributed also to the fact that the k–ε model is not sensitized to the implicit effects of rotation on turbulence. To our knowledge, Chung and Sung [11] were the first to perform LES in a Taylor-Couette-Poiseuille system. They compared their numerical data to the experimental ones of Nouri and Whitelaw [8] for $\eta = 0.5$, $C_w = 20\ 970$, and $Re = [954.5; 1909.1; 3818.1]$. They obtained a relatively close agreement for the mean velocity and the Reynolds stress tensor components. The mean tangential velocity is slightly overestimated in the main part of the radial gap between the cylinders. They focused their numerical investigation on

the appearance of turbulent structures attributed to the destabilization of the flow along the inner rotating cylinder and giving rise to strong events (sweeps and ejections).

The reader can refer to the recent works of Kuosa *et al.* [12] and Poncet *et al.* [13] for computations in a Taylor-Couette-Poiseuille flow with heat transfer effects. Kuosa *et al.* [12] considered the cooling of high-speed electrical machines, where only the inner cylinder is rotating. They compared the predictions of three different models: an algebraic modeling, a low Reynolds number k–ε modeling and a k–ω SST model. The hydrodynamic and thermal fields are established for various rotation rates and mass flow rates. The three turbulence models underestimated the heat transfer coefficients along both cylinders. Moreover, the entrainment coefficient of the fluid was far from the theoretical value for a fully turbulent flow. These discrepancies were attributed by the authors to the boundary conditions imposed at the inlet and outlet sections and to the turbulence models used. Poncet *et al.* [13] proposed some calculations using the Reynolds Stress Model of Elena and Schiestel [14] in the rotor–stator gap of an electrical motor for real operating conditions. This model improves the predictions of Naser [10] in the isothermal case and predicts quite well the velocity fluctuations apart close to the outer cylinder. They performed also a parametric analysis of the flow and temperature fields for a wide range of Reynolds and Prandtl numbers and flowrates.

The paper is organized as follows: the geometrical configuration and the numerical modelings are described in Sections 2 and 3 respectively. The numerical benchmarking is performed in Sections 4 and 5 on two well documented test cases: the closed Taylor-Couette system of Burin *et al.* [1] in Section 4 and the experimental set-up of Escudier and Gouldson [2] in Section 5. Finally some conclusions and closing remarks are provided in Section 6.

## 2. Geometrical configurations

Two Taylor-Couette configurations have been considered in the following. For both systems, the fluid is confined between two concentric cylinders of radii $R_1$ and $R_2$ and height $H$ (Fig.1). The inner cylinder is rotating at a constant angular rate $\Omega$, while the outer cylinder is stationary. The originality of the first apparatus developed by Burin et *al.* [1] is that each endcap is divided into two independently driven rings of equal radial extension. The inner cylinder and the inner ring rotate at $\Omega$, while the other walls are stationary. The second case corresponds to the experimental set-up developed by Escudier and Gouldson [2]. The cavity is then opened so that an axial Poiseuille flow (volumetric flowrate denoted $Q$) can be superimposed to the base Taylor-Couette flow. In the following, the radial and axial coordinates are normalized as: $r^* = (r-R_1) / (R_2-R_1)$ and $z^* = z / H$.
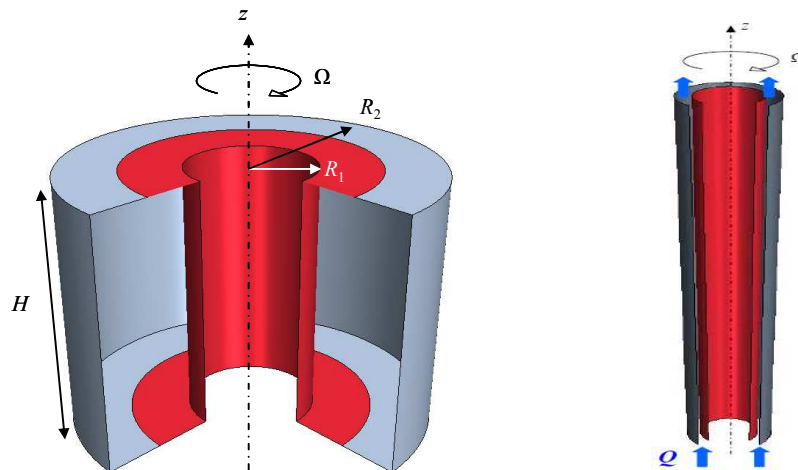


Figure 1: Geometrical configurations corresponding to the systems considered by Burin *et al.* [1] on the left and by Escudier and Gouldson [2] on the right. Red walls are rotating and grey ones are stationary.

For both systems, the main flow is governed by four flow control parameters:
- the rotational Reynolds number $Re = \Omega R_1 (R_2-R_1) / v$ based on half the hydraulic diameter $D_H/2 = R_2-R_1$,
- the volumetric flowrate coefficient $C_w = Q / (v R_2)$,
- the aspect ratio of the cavity $\Gamma = H / D_H$ and
- the radius ratio $\eta = R_1 / R_2$.

The values of these parameters are summed up in Table 1 for the two test cases. In both cases, the radius ratio remains in the range $0.33 < \eta < 0.67$, so that the cavity is considered as a middle gap cavity [15]. For enclosed systems characterized by a low aspect ratio $\Gamma$, such as in the experiment of Burin *et al.* [1], the choice of the boundary conditions on the endcap disks is primordial and can favour the development of large Ekman recirculations.

Table 1: Flow control parameters

| Test case | $\Gamma$ | $\eta$ | Re | $C_w$ |
|---|---|---|---|---|
| 1-Burin *et al.* [1] | 1.06 | 0.35 | 100 000 | 0 |
| 2-Escudier & Gouldson [2] | 116 | 0.506 | 948.3 | 17500 |

## 3. Numerical methods

Table 2: Computational details

| | Test case | δt (s) | NPR x NPA x NPZ | total number of mesh points | mesh type | wall coordinates | Time per iteration (s) | geometry | platform |
|---|---|---|---|---|---|---|---|---|---|
| RSM [14] | 1 | 0.01 | 140 x 1 x 280 | 39 200 | Structured mesh | r+<0.02 z+<0.06 | 16 | 2D axisymetric | M2P2 cluster with 2 xeon quadcore 3 GHz |
| | 2 | steady | 180 x 1 x 400 | 72 000 | | r+<0.3 z+<1.1 | 2.4 | | |
| DNS | 1 | 0.00003 | 152 x 64 x 242 | 2 354 176 | Structured mesh | r+<4 z+<6 | 17.2 | 3D (half cavity) | M2P2 cluster with 2 xeon quadcore 3 GHz |
| Unsteady k-ω SST (OpenFOAM) | 1 | 0.0004 | 140 x 5 x 280 | 196 000 | multi-block hexahedral grid | r+<5 z+<150 | 4.5 | 2D axisymetric (1° sector) | 2 cores of an Intel Xeon 3430 at 2.40GHz |
| LES (OpenFOAM) | 1 | | | | | | 8.5 | 3D (90° sector) | 6 cores of an Intel Xeon 3430 at 2.40GHz |
| | 2 | 0.0015 | 180 x 70 x 300 | 3 780 000 | | r+<6 z+<200 | 4.5 | | 2 cores of an Intel Xeon 3430 at 2.40GHz |
| SAS-SST (CFX) | 1 | 0.00005 | 140 x 5 x 280 | 196 000 | multi-block hexahedral grid | r+<5 z+<5 | 30 | 2D axisymetric (5° sector) | In parallel on 4 cores of an Intel Xeon 3430 at 2.4 GHz |
| v2-f (StarCCM+) | 1 | 0.01 | 74 x 104 x 115 | 4 117 637 | Polyhedral unstructured mesh with prismatic layers along the walls | r+<0.3 z+<0.5 | 17.6 | 3D | HP Z400 workstation with a quadcore Intel Xeon CPU W3520 processor of 2.67 GHz |
| | 2 | 0.01 | 54 x 84 x 240 | 2 853 705 | | r+<1.3 z+<2.15 | 19.1 | | |
| RSM (StarCCM+) | 1 | 0.01 | 74 x 104 x 115 | 4 117 637 | | r+<0.15 z+<0.35 | 30.1 | | |
| | 2 | 0.005 | 54 x 84 x 240 | 2 853 705 | | r+<0.3 z+<0.5 | 31.3 | | |
| DES (StarCCM+) | 1 | 0.005 | 74 x 104 x 115 | 4 117 637 | | r+<1.2 z+<2.15 | 15 | | |
| | 2 | 0.005 | 54 x 84 x 240 | 2 853 705 | | r+<0.6 z+<1.65 | 18 | | |
| LES (StarCCM+) | 1 | 0.001 | 74 x 104 x 115 | 4 117 637 | | r+<0.7 z+<0.95 | 13.4 | | |
| | 2 | 0.001 | 54 x 84 x 240 | 2 853 705 | | r+<1.2 z+<2 | 16.6 | | |

Different numerical approaches including RANS, DES and LES models either developed at the M2P2 laboratory, by the HTC group at the University of Florence or available within commercial codes have been compared in the two configurations. All the numerical approaches together with the corresponding computational details are summed up in Table 2. A brief description of the various numerical methods employed is given in the following. Note that NPR, NPA and NPZ represent the number of mesh points in the radial, tangential and axial directions respectively.

## 3.1 Direct numerical simulation

Conservation equations are solved using a Fourier approximation in the homogeneous tangential direction. In both non homogeneous radial and vertical directions the solutions are approximated using a fourth-order compact finite-difference scheme [16]. The time advancement is second-order accurate and is based on the explicit Adams–Bashforth time-stepping for the convective terms and an implicit backward-Euler scheme for the viscous terms. The velocity-pressure coupling is solved using a two-step fractional scheme (predictor–corrector) reducing the problem at each time step to a set of two-dimensional Helmholtz equations. The cartesian solver has been fully validated in [17] and in [16] for the multidomain version. The numerical validation of the cylindrical solver has been done by Viazzo *et al.* [18] in an interdisk rotor-stator cavity. It is noteworthy that, for the Burin *et al.*'s case, the calculation domain has been divided into four subdomains (two in each radial and axial directions) to take into account the singularity between the endcap rings.

## 3.2 Reynolds Stress Model (RSM) of Elena & Schiestel [14]

This innovative RSM is a low Reynolds number second-order full stress transport closure sensitized to rotation effects by Elena and Schiestel [14]. Four terms compared to the former model of Launder and Tselepidakis [19] have been added in this version. They account for the implicit effects of rotation on turbulence and act only when the flow is subjected to strong rotation. The first term $\Phi^{(R)}$ is a part of the pressure-strain correlation term sensitized to the dimensionality tensor $C_{ij}$. The second term $D^R$ is an inhomogeneous diffusion term, which slows down the tendency to bidimensionalization for wall bounded flows. The third term $B_{ij}$ is a homogeneous source term, which rectifies the pressure-strain correlation and which acts only in case of strong rotation. It produces spectral phase scrambling (angular dispersion). The rotation also reduces the energy transfer from large to small turbulent scales; this phenomenon is modeled through an inverse flux $J_{ij}$ considered as isotropic for high Reynolds number. It is a correction term of the dissipation $\varepsilon_{ij}$, which increases the turbulence levels in the core of the flow. The dissipation rate equation $\varepsilon$ is the one proposed by Launder and Tselepidakis [19]. More details can be found in [14, 20].
The RSM has been implemented in a finite-volume code using staggered grids for mean velocity components with axisymmetry hypothesis in the mean and non staggered grids for the Reynolds stress tensor. The velocity-pressure coupling is solved using the SIMPLER algorithm. In order to overcome stability problems, several stabilizing techniques are introduced in the numerical procedure. The stress component equations are solved using matrix block tridiagonal solution to enhance stability using non staggered grids.

## 3.3 LES and URANS models within OpenFOAM

OpenFOAM is an open-source CFD code composed of a set of libraries implemented to resolve continuum mechanics problems in 3D on unstructured grids [21, 22]. The results for the cases of interest were obtained exploiting pressure based segregated incompressible solvers implementing SIMPLE algorithm for the steady-state and PISO for the transient computations. Both the convective and diffusive flux schemes employed are based on a purely linear interpolation, time advancement is achieved by means of the implicit backward Euler scheme, guaranteeing second order accuracy both in space and in time. For the unsteady calculations both RANS and LES turbulence modeling have been compared on the same computational grids. The time step was generally chosen to guarantee a maximum Courant number inside the domain close to unity to guarantee stability and improve the convergence rate. The RANS calculations have been conducted with a low-Reynolds k-ω SST turbulence closure [23] exploiting blended second and first order discretization for the convective schemes while the LES subgrid effects are evaluated by means of a one-equation model implementing a transport equation for the modeled turbulence kinetic energy [24, 25].

## 3.4 k-ω SST and SAS SST models within CFX

The calculations performed using CFX are unsteady isothermal solutions. The time step have been selected assuring, for each operating velocity, an RMS Courant number lower than 1. The evolving fluid is considered ideally

incompressible with constant transport properties. The convective fluxes were solved using a high order resolution scheme. Two turbulence models have been considered. The first one is the well know k-ω SST while the second one is the innovative SST SAS originally proposed by Menter and Egorov [26]. The Scale-Adaptive Simulation (SAS) is an improved URANS formulation, which allows the resolution of the turbulent spectrum in unstable flow conditions. The SAS concept is based on the introduction of the von Karman length-scale into the turbulence scale equation. The information provided by the von Karman length-scale allows SAS models to dynamically adjust to resolved structures in a URANS simulation, which results in a LES-like behavior in unsteady regions of the flow field. At the same time, the model provides standard RANS capabilities in stable flow regions. The governing equations of the SST SAS model differ from those of the SST RANS model by an additional source term in the transport equation for the turbulence eddy frequency. Further details regarding the SST SAS model are available in the literature [26, 27]. Automatic wall treatment (i.e. automatic blending from low to high Reynolds treatment as a function of the local first node wall distance) have been considered for both models.

## 3.5 URANS, DES and LES using Star CCM+

Different models available in Star CCM+ 5.04 have been also compared for the two test cases. Many classical RANS models (k-ε, k-ω SST…) have been considered including both high and low-Reynolds number approaches but we will focus in the following only on the four approaches, which provide the best overall agreement: a k-ε $v^2$-f model, a RSM model, a Detached Eddy Simulation (DES) based on the Spalart-Allmaras model and a Large Eddy Simulation based on the standard Smagorinsky subgrid scale model [28].

The $v^2$-f model is optimized to capture the near-wall turbulence effects more accurately, which is crucial for the accurate prediction of heat transfer, skin friction and flow separation. It solves two additional turbulent quantities compared to standard k-ε models, namely the normal stress function and the elliptic function, in addition to $k$ and $\varepsilon$. This model is designed to handle wall effects in turbulent boundary layers and to accommodate non-local effects.

The RSM model available within Star CCM+ is the same as the one developed by Elena and Schiestel [14] without the specific terms of rotation and the LES model uses a standard Smagorinsky as subgrid scale model with a model constant $C_s$ equal to 0.1.

The DES version of the Spalart-Allmaras model solves a transport equation to determine the turbulent viscosity. As for the SAS-SST model previously presented, the DES has a LES-like behaviour in unsteady regions of the flow field, while preserving standard RANS capabilities in stable flow regions.

## 4. Taylor-Couette flows in a closed cavity with endcap effects

Burin *et al.* [1] developed an original Taylor-Couette system with two independent end-rings between the inner and outer cylinder dedicated to the study of fluid angular momentum transport. Compared to classical Taylor-Couette systems, these rings seem to allow for a reduction of the Ekman circulation and to create a Couette-like velocity profile: $V_\theta(r) \propto 1/r^2$. They provided useful data for comparisons in terms of mean and turbulent quantities.
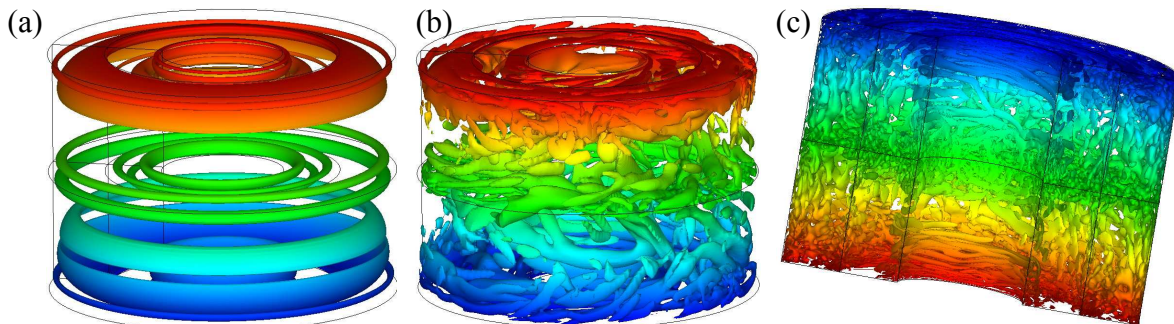
## 4.1 Flow structures



Figure 2: Iso-values of *Q*-criterion colored by the axial coordinate $z^*$ obtained by DNS: (a) *Q=5* for *Re=3000*, (b) *Q=50* for *Re=10⁴* and (c) *Q=5000* for *Re=10⁵*.

The critical Reynolds number *Re* for the transition to turbulence in such a flow depends upon a number of factors, including the aspect ratio of the cavity, the curvature and the flow history but the commonly admitted value is around $10^5$. In the present case, the transition to a state of featureless turbulence appears for lower values of *Re*. At very low

*Re* values, the flow is laminar unstable with some circular rolls of different sizes propagating towards the gap (Fig.2a). They are somewhat different from classical Taylor vortices, which would have occupied the whole cavity with a corresponding axial wave number of *2* (close to *2Γ*). At *Re=10⁴*(Fig.2b), some spiral patterns aligned with the tangential direction appear along the inner rings and around the midplane $z^*=0.5$. Some evidence of a disorganized flow structure can be seen from the Q-criterion map. When one increases further the Reynolds number, the flow gets clearly turbulent at *Re=5.10⁴* (not shown here) with a similar flow pattern as the one shown in Figure 2c for *Re=10⁵*. At *Re=10⁵*, the iso-values of the Q-criterion obtained by DNS (Fig.2c) show indeed that the flow is clearly turbulent with thin turbulent structures aligned with the rotation axis. There is absolutely no evidence of large scale vortical structures embedded in the flow apart from large circular patterns, which appear along the inner cylinder. Turbulence is mainly concentrated at midplane ($z^*=0.5$) because of the shear produced by the intense recirculation bubbles (Fig.4). Thus, the critical Reynolds number for the transition to turbulence is clearly reduced by the presence of the endcap rings compared to classical Taylor-Couette flows.
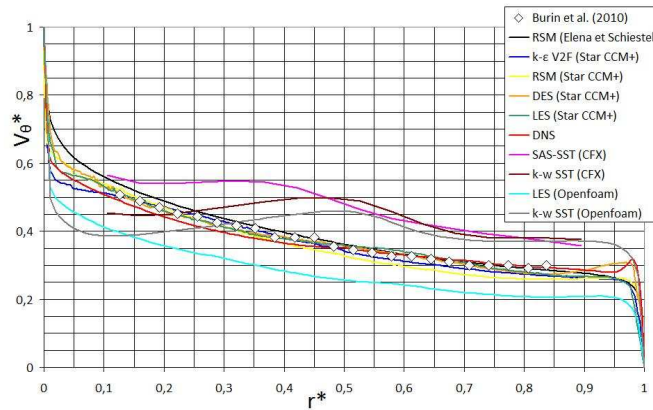
## 4.2 Averaged mean and turbulent fields



Figure 3: Radial profiles of the mean tangential velocity at $z^*=1/4$.

All the computed data have been averaged both in time and in the tangential direction. Figure 3 presents the radial profiles of the mean tangential velocity component $V_\theta^* = V_\theta / (\Omega R_1)$ at the axial position $z^*=1/4$. From the experimental values and most of the numerical approaches (apart from the k-ω SST and the SAS models), the flow is clearly divided into three areas. Two very thin boundary layers develop along the cylinders with a thickness of the order of 1% of the gap width. They are separated by a central region where the tangential velocity component scales like: $V_\theta^*(r) = 0.209+0.0025/r^2$, which is typical of Taylor-Couette flow profiles. Whatever the solvers (StarCCM+, CFX or OpenFOAM), the k-ω SST model fails to predict the expected profile with a non monotonous behaviour and a large overestimation of the mean tangential velocity. For all the models, $V_\theta^*(r^*=0.5)$ is equal to *0.35*, whereas the LES model within OpenFOAM predicts a much lower value *0.25*. It is noteworthy that the DNS as well as the DES predict a local maximum close to the outer cylinder but due to the lack of experimental data very close to the wall, no definitive conclusion can be drawn.
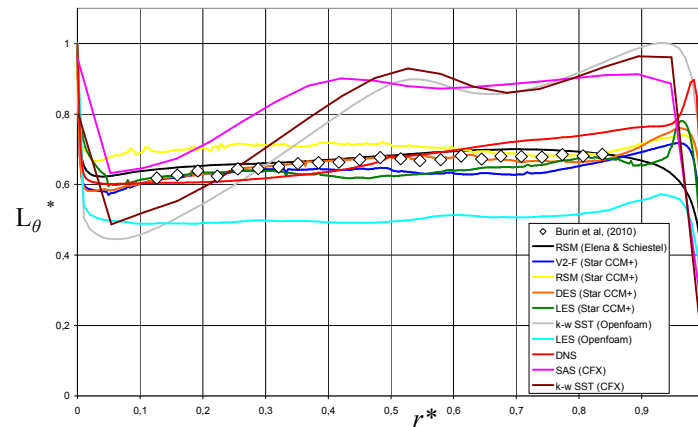


Figure 4: Radial profiles of the normalized angular momentum at $z^*=1/4$.

Figure 4 presents the radial profiles of the angular momentum $L_\theta = r\,V_\theta$ of the mean flow at the same axial location. It has been made dimensionless using the value of $L_\theta$ at the inner cylinder $L_\theta (R_1) = \Omega R_1^2$. Apart very close to the walls where no experimental data are available, the angular momentum slightly increases with the local radius. The value at mid-gap is around *0.65*, which is much larger than the usual value *0.5* obtained in classical Taylor-Couette flows [29]. It can be explained by considering the additional torque from the inner rotating rings, which rotate at the same rate as the inner cylinder but at a larger radius. Even if most of the models predict quite well the mean tangential velocity, the variations of the angular momentum with the radius highlight larger discrepancies mainly because of the normalization. The DNS slightly overestimates the slope of the profile in the central region, where the RSM of Elena and Schiestel [14] offers the best agreement with the experimental data of Burin *et al.* [1]. The $v^2$-f model provides also quite good results for the mean field.
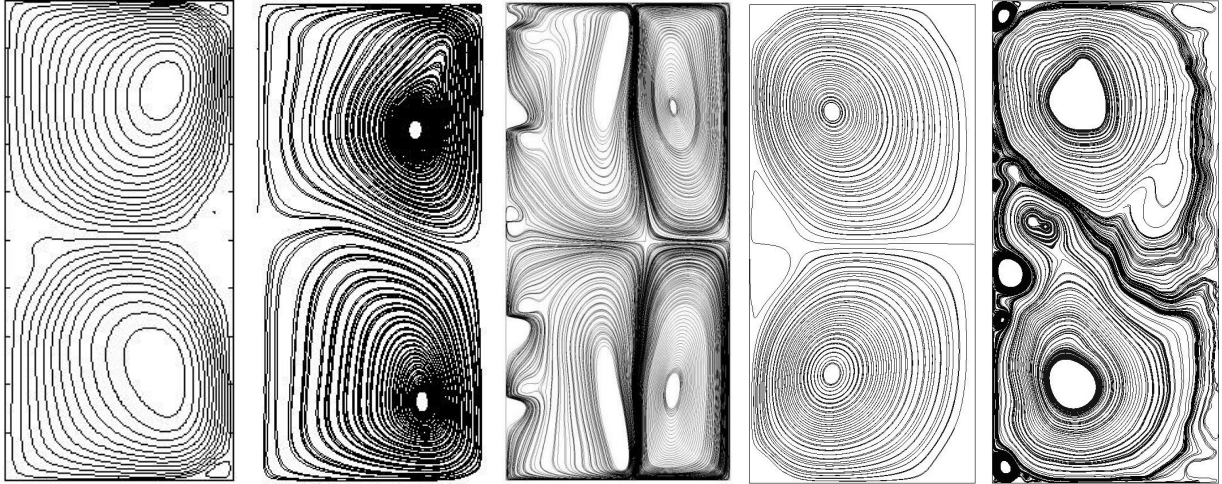


Figure 5: Streamline patterns obtained, from the left to the right by the RSM [14], the RSM (StarCCM+), the SAS-SST (CFX), the LES (OpenFOAM) / mean streamlines and the LES (OpenFOAM) / instantaneous streamlines. The rotation axis is on the left of each subfigure.

The computed streamline patterns obtained by some numerical approaches are displayed in Figure 5. The SST SAS model predicts a mean velocity pattern characterized by four rotating structures at the meridian plane, which is confirmed by the steady or unsteady versions of the k-ω SST model within CFX (not shown here). This evidence is in contrast with what emerges from the RSM and LES calculations that predict just two large counter-rotating vortices. In the SST computations the fluid pumped along the rotating disk is deviated away from the wall almost as soon as it reattaches on the fixed ring creating a high tangential velocity zone around mid-radii. Such movement towards the center of the cylinder creates two counter rotating bubbles in the inner and outer zone. While the outer bubble is almost axisymmetric, the inner one is centered quite close to the rotating disk showing a quite stretched shape. For the LES predictions instead the fluid moving towards the outer cylinder close to the rotating disks is not blocked by the fixed ring and continues to flow in the radial direction before bending towards the center of the cylinder due to a vortex arising in the corner between the two stationary walls. Similarly another vortex appears between the two main bubbles close to the outer cylinder. It is also possible to note smaller vortical structures along the inner cylinder both by the SST and LES. They are formed close to mid height of the cylinder and are convected towards the rings. The unsatisfying agreement with the experimental data provided by Burin *et al.* [1] in terms of tangential velocity is probably related to the presence of the four rotating structures on the meridian plane. The velocity peak close to the radius $r^*=0.35$ on Figure 3 can be indeed justified by the tangential momentum transport operated by these inner vortices.

Some comparisons have also been performed for the turbulent field in terms of the cross correlation coefficient of the relative fluctuations $C_{r\theta}$ and of the turbulent angular momentum transport $G$ defined as:

$$C_{r\theta} = \frac{\left\langle v_\theta' v_r' \right\rangle}{\left\langle v_\theta' \right\rangle_{rms} \left\langle v_r' \right\rangle_{rms}} \qquad\qquad G = \frac{2\pi r^2 \left\langle v_\theta' v_r' \right\rangle}{v^2}$$

Burin *et al.* [1] provided the variations of these two coefficients with the Reynolds number *Re*. They observed that $C_{r\theta}$ slightly decreases with *Re* as the flow becomes increasingly random. As it can be seen from Figure 6a, the time averaged value obtained by the different models at the monitoring point is close to 20% and does not vary so much with *Re* in the range [*500, 4.10$^5$*], in quite good agreement with [1]. For *Re=5×10$^4$*, Smith and Townsend [29] found $C_{r\theta}$=30-40%. This value is confirmed by the numerical results of the RSM (StarCCM+), whereas all the other approaches predict $C_{r\theta}$=0.24 or less. The high value obtained by [29] is due, according to [1], to the presence of large scale vortical structures embedded in the flow, which has not been observed here by none of the present models. In fact, this coefficient strongly varies between *-0.4* and *0.4* depending on the computed position as it can be seen from the $C_{r\theta}$–map in Figure 6b obtained by LES (OpenFOAM) in a meridian plane. Thus, those punctual values cannot be considered representative of the time averaged cross correlation in that region.
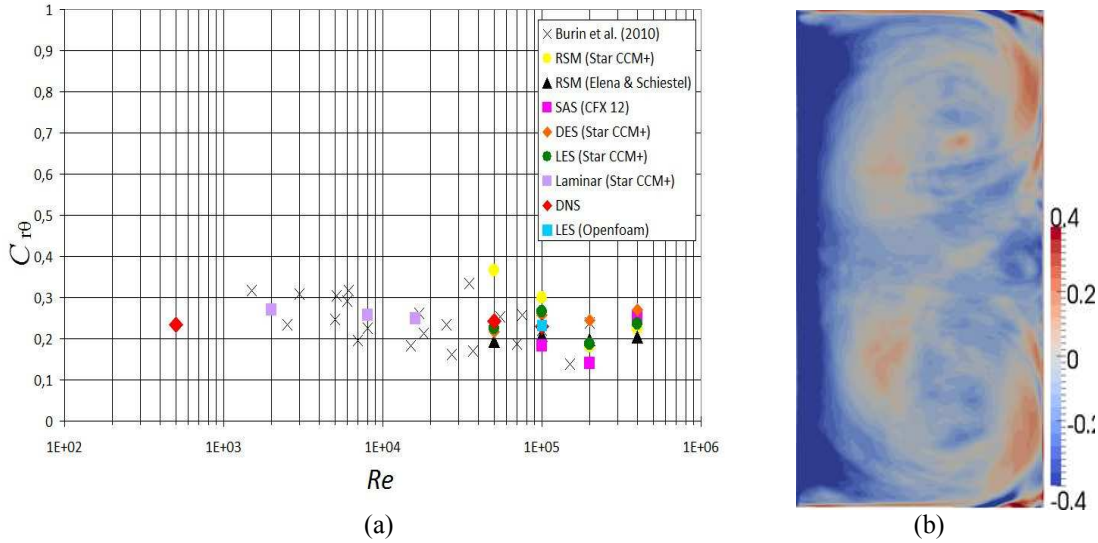


(a)



(b)

Figure 6: (a) Variations of the cross correlation coefficient $C_{r\theta}$ with the Reynolds number *Re* at $z^*$=1/4 and $r^*$=3/4; (b) Map of $C_{r\theta}$ in a meridian plane obtained by the LES (OpenFOAM).
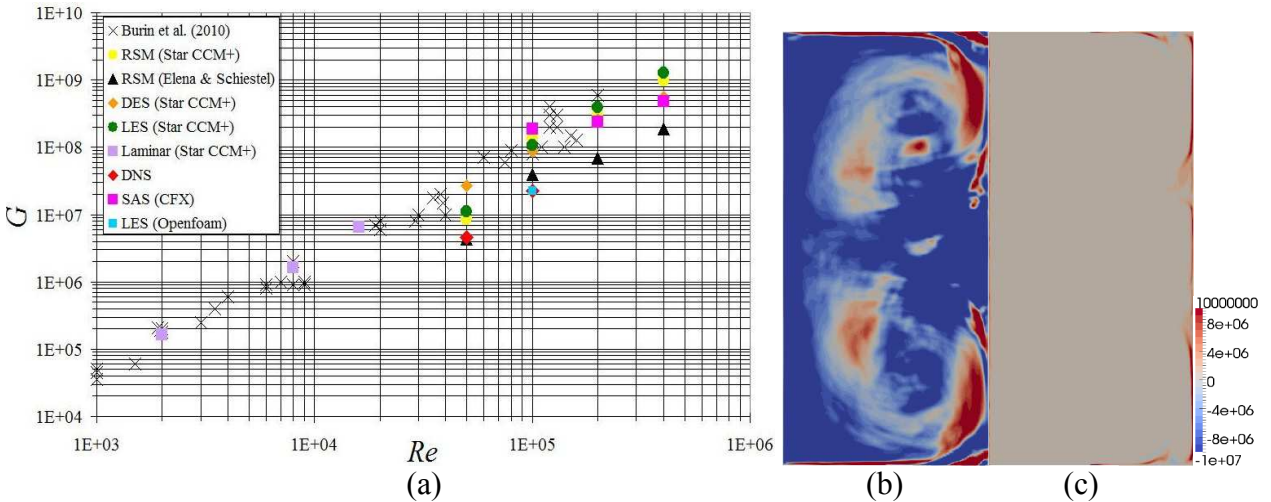


(a)



(b)          (c)

Figure 7: (a) Variations of the non-dimensional turbulent angular momentum transport *G* with the Reynolds number *Re* at $z^*$=1/4 and $r^*$=3/4; Maps in a meridian plane of the (b) resolved and (c) modelled parts of *G* obtained by LES (OpenFOAM).

In Figure 7, the measured velocity correlation is discussed in terms of a dimensionless torque per unit length *G* (in which the viscous term has been neglected as in [1]). Its variation with the Reynolds number is shown in Figure 7a for all the approaches and compared to the measurements of [1]. Laminar computations using StarCCM+ have also been performed to extent the range of *Re*-values. For high *Re* values, the DES results confirm that *G* depends on *Re*

9

following a power law: $G \propto Re^{\alpha}$ with $\alpha=1.7$ in good agreement with the measurements of Wendt [4]. For lower values, the laminar calculations provide: $\alpha=1.6$. Considering the whole range of $Re$, we finally found $G \propto Re^{1.65}$, which matchs the previous results of [1, 30]. All the models provide the same trend as the experiments even if most of them (both LES, the RSM [14] and the DNS) underestimate the values of $G$. Looking at Figure 7b, one may also argue whether comparing a punctual value is an efficient strategy to verify turbulence levels when, as this is the case here, the local variability of the resolved part of $G$ is high. Figure 7c shows how the modeled contributions are important only very close to the outer walls and are of the same order of magnitude as the resolved part in that regions.

A preliminary calculation on a 1° sector using the LES within OpenFOAM has been performed providing much lower values of both $C_{r\theta}$ and $G$ with at least one order of magnitude. This finding confirms the importance of large tangential vertical structures on the behaviour of the flow.

## 5. Taylor-Couette-Poiseuille flows in an opened cavity

A second test case is considered corresponding to the large aspect ratio Taylor-Couette system developed by Escudier and Gouldson [2] in which an axial Poiseuille flow is supplied to the cavity (see Table 2 for the flow parameters). Most of the models used for comparisons in the previous case are tested for this case as well.

### 5.1 Flow structures

In order to offer an idea of the turbulent structures arising in the flow, maps of the instantaneous tangential and axial velocities are reported in Figures 8b & 8c respectively together with the isovalues of the Q-criterion in Figure 8a obtained by LES (OpenFOAM). Note that the isocontours of $Q$ are reported from the point where turbulent flow behaviour first arises, due to the laminar behavior imposed by the inflow boundary condition, at approximately one-fourth of the entire axial extension.
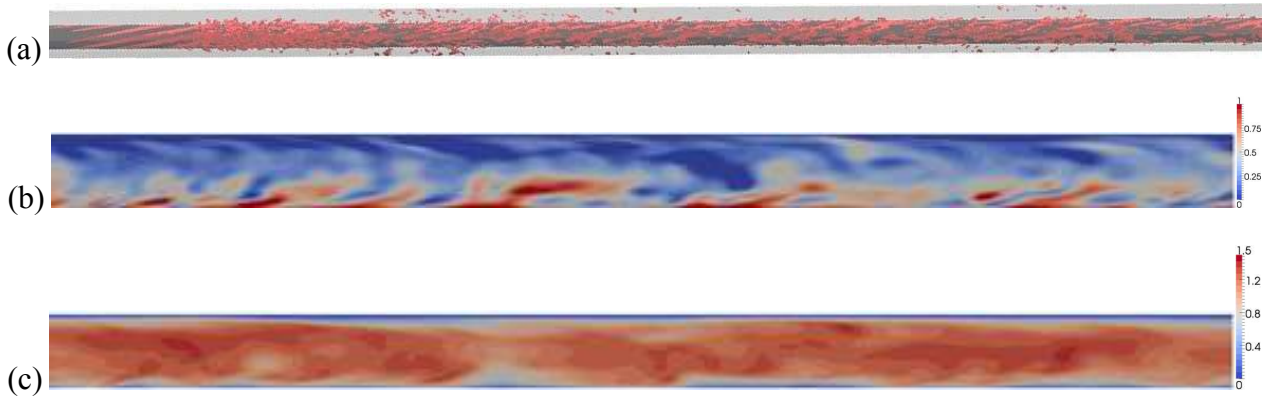
(a)



(b)



(c)



Figure 8: (a) Iso-values of $Q$-criterion ($Q=-2000$) and maps of the instantaneous (b) tangential and (c) axial velocity components in a meridian plane (the rotation axis is at the bottom of each figure and it flows from the left to the right). Results obtained by LES using OpenFOAM.

The radial velocity component (not reported here) is almost zero in the whole cavity for this set of parameters. Thus, the flow is a combination of an intense Taylor-Couette flow close to the inner rotating cylinder due to rotation (Fig.8b) and of an axial Poiseuille flow within the gap (Fig.8c). It explains the presence of helical vertical patterns, which roll up along the inner wall (Fig.8a). Otherwise there is no evidence of 3D large scale structures embedded in the flow. The main flow is dominated by the axial Poiseuille flow, which can be explained by the low value of the rotation parameter $N = \Omega R_1 / \overline{V}_z = 0.148$ .

### 5.2 Averaged mean and turbulent fields

The predictions of the RSM [14] and other models available within OpenFOAM and StarCCM+ are compared to the LDA measurements of Escudier and Gouldson [2] at a given axial position $z^* = 0.1$ and to the previous k-ε computations of Naser [10]. The mean tangential velocity component is normalized using the rotational speed of the inner cylinder $\Omega R_1$, whereas the mean axial velocity component is normalized using the mean axial velocity $\overline{V}_z$

imposed at the inlet, defined by $\overline{V}_z = Q/[\pi(R_2^2 - R_1^2)]$: $V_\theta^* = V_\theta/(\Omega R_1)$ and $V_z^* = V_z/\overline{V}_z$. To enable direct comparisons with the measurements, the tangential $v'_\theta$ and axial $v'_z$ normal stresses are normalized by $\overline{V}_z$: $v_\theta^{'*} = \sqrt{\overline{v_\theta^{'2}}}/\overline{V}_z$ and $v_z^{'*} = \sqrt{\overline{v_z^{'2}}}/\overline{V}_z$.

As it can be seen from Figure 9a, the tangential velocity varies with *1/r* within the gap apart close to the walls where two boundary layers develop. The tangential velocity profile is quite far from the laminar circular Couette profile: $V_\theta(r) \propto 1/r^2$ highlighting the turbulent nature of the flow. The boundary layer thicknesses are here much thicker ($\approx$ 15% of the gap width each) than in test case 1, because of a lower value of the rotation rate $\Omega$. Most of the computed results are found in good agreement with the experimental data for the mean tangential velocity. The DES and most of all the RSM [14] and the k-ω SST of OpenFOAM provide the best results. On the contrary, the LES and RSM of StarCCM+ predict a centerbody rotation within the gap with an overestimation of the mean tangential velocity whatever the radial position is, leading to around 17% of error at *r*=0.5*. This behaviour is characteristic to higher values of the rotation parameter *N* as depicted in [13].
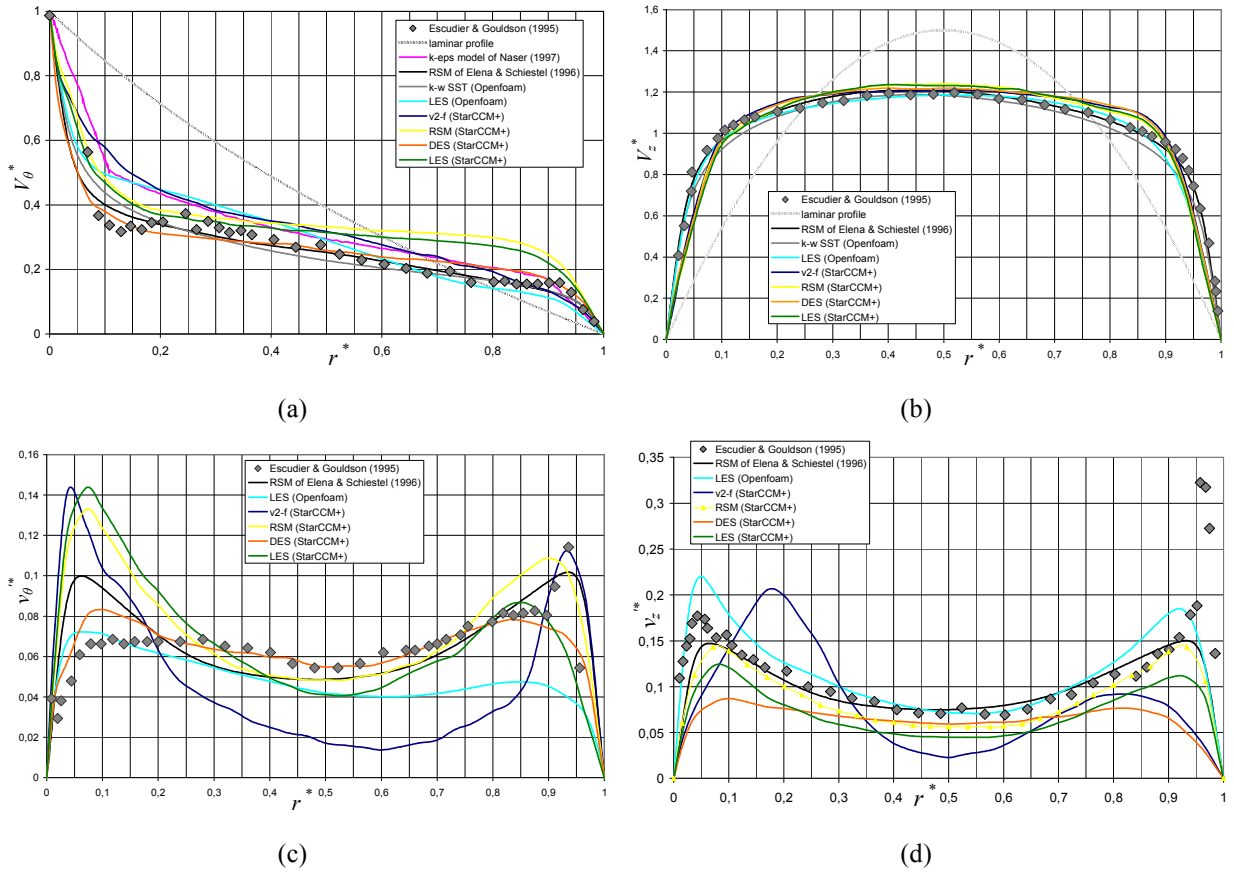


(a)



(b)



(c)



(d)

Figure 9: Radial profiles of the mean (a) tangential and (b) axial velocity components and of the corresponding fluctuating (c) tangential and (d) axial velocity components at $z^*=0.1$.

The radial variations of the mean axial velocity component displayed in Figure 9b confirm the turbulent nature of the flow by comparison with the laminar Poiseuille profile. The results of the LES, the k-ω SST (OpenFOAM) and the RSM [14] predict the same symmetric profile as in the experiments of [2]. All the other approaches found in StarCCM+ overestimate the axial velocity in the bulk of the flow and by conservation of mass, they overestimate also the boundary layer thicknesses. The results obtained by Naser [10] are not shown here as surprisingly, mass is not conserved. It is noteworthy that fully developed conditions are reached at $z^* = 0.1$ using the RSM, for example, in agreement with the observations of Escudier and Gouldson [2], whereas the predictions of the k-ε model of Naser [10] showed a large dependence of the mean velocity profiles on the axial position. This last author attributed the discrepancies obtained by the k-ε model to the fact that its model is blind to any rotation effects, and that the eddy viscosity concept, on which this model is based, is unsuitable with the present flow situation. On the contrary, the

11

present RSM model is both sensitized to rotation effects [14] and free from any eddy viscosity hypothesis, which may explain the better overall agreement with the experimental data.

Another calculation on a 1° sector using the LES within OpenFOAM has also been performed but not shown here. The 90° set-up for the LES calculation shows a strong improvement in reproducing turbulent velocity profiles, whereas the profile of axial velocity obtained by the 1° sector LES is fairly close to the classical laminar Poiseuille profile with a much higher maximum velocity at mid-gap.

Figures 9c & d present the radial distributions of the tangential and axial normal Reynolds stress tensor components for the same set of parameters. Turbulence is mainly concentrated in the core region with peak values at the edge of each boundary layer. Then, it vanishes towards the walls. Turbulence intensities are much higher close the outer cylinder as it can be seen from the experiments of [2], which is not captured by any of the numerical approaches. This behaviour observed in the experiments looks surprising. The same authors report indeed similar measurements in [31] for another value of $C_w = 16\ 672$ very close to the present one. In that case, the profile of the fluctuating axial velocity is almost symmetric, with values remaining lower than $0.2$. The values around $0.35$ in Figure 9b may be attributed in the experiments to the difficulty to perform accurate measurements very close to the walls. The RSM of Elena & Schiestel [14] provides the best overall agreement with good intensity levels in the gap and close to the inner cylinder. The LES of OpenFOAM offers also quite good results excepted for the $v_\theta^{'*}$ intensity at large radial locations.

The reader can refer to [13, 20] for more comparisons with other classical RANS models and other computations for three values of the flowrate coefficient.

## 6. Conclusion

Numerical predictions have been performed using a DNS code, the RSM closure of Elena & Schiestel [14] and some LES, DES and RANS models available within OpenFOAM, StarCCM+ or CFX. The computed results have been compared to experimental data available in the literature for two different Taylor-Couette flow arrangements: the original set-up of Burin *et al.* [1] characterized by endcap rings enclosing the cavity and the experiment of Escudier and Gouldson [2], for which an axial Poiseuille flow is superimposed to the circular Couette base flow.

In the enclosed cavity of Burin *et al.* [1], the difficulty arises from the presence of two endcap rings attached to both cylinders. It appeared then crucial to take into account accurately the brutal variations in the boundary conditions on the upper and lower walls. A multidomain DNS code has then been developed providing in that case very valuable data for comparisons with the experimental data and other numerical results. DNS showed that there is no evidence of Taylor vortices embedded in the turbulent flow apart very close to the inner cylinder where circular vortices have been observed. It explains why the 2D unsteady RSM [14], which has been sensitized to the implicit effects of rotation on turbulence, provides the best overall agreement in that case, where the rotation rate is quite high. On the contrary, all the SST models including the innovative SAS SST model fail to predict the mean tangential velocity profiles with large discrepancies even in the core of the flow. It can be attributed to the existence of four large recirculations in a meridian plane, whereas all the other models predict only two bubbles. The DES matches quite well also with the measurements [1]. All the models predict the good tendency for the turbulent angular momentum transport $G$, which is found to vary as $Re^{1.65}$ in agreement with previous approaches [1, 4, 29, 30]. Nevertheless, most of the models including the RSM [14], the LES (OpenFOAM) but also the DNS underpredict the shear stress tensor component $v_r' v_\theta'$. The cross correlation coefficient $C_{r\theta}$ is well predicted by all the approaches with almost a constant value around $0.2$ (at a given location) for a wide range of Reynolds numbers. The LES provides very useful data showing the high variability of these two parameters.

Some comparisons have been also performed in a very elongated Taylor-Couette system with an imposed axial Poiseuille flow. LES computations within OpenFOAM have shown first that there is still no 3D patterns embedded in the flow. For this set of parameters, the DES (StarCCM+), LES (OpenFOAM) and RSM [14] have been very favourably compared to the velocity measurements of Escudier and Gouldson [6]. In particular, they improve significantly the predictions of the k-ε model of Naser [10] for the mean velocity distributions. All models predict quite well the mean field with a tangential velocity inversely proportional to the radial location. The $v^2$-f and LES of StarCCM+ predict a constant tangential velocity, which is usually characteristic of higher rotation parameters. Even if they do not predict the asymmetry of the fluctuating velocity profiles, the turbulence intensities in the core region computed by the DES, LES and RSM [14] are in good agreement with the experimental data. None of the tested models predict the peak values obtained very close to the outer cylinder.

For industrial applications, the $v^2$-f model showed a good behaviour in these two test cases providing good results for the mean field. It offers then a good compromise between accuracy and calculation cost. For more specific applications where turbulence intensities have to be computed accurately, the RSM [14], which has been sensitized to the main rotation effects, has shown to predict quite accurately both the mean and turbulent fields. Other calculations are now required in another configuration where three-dimensional effects can arise and affect the mean and turbulent fields to test then the superiority of the LES approaches.

## References

[1] Burin, M.J., E. Schartman and H. Ji. 2010. Local measurements of turbulent angular momentum transport in circular Couette flow. *Exp. Fluids* 48: 763-769.

[2] Escudier, M.P. and I.W. Gouldson. 1995. Concentric annular flow with centerbody rotation of a Newtonian and a shear-thinning liquid. *Int. J. Heat Fluid Flow* 16: 156-162.

[3] Owen, JM. 2000. Flow and heat transfer in rotating disc systems. 2000. In *CHT01 Turbulence Heat and Mass Transfer 3*, ed. Y. Nagano, K. Hanjalic, T. Tsuji, pp. 33–58. Tokyo: Aichi Shuppan.

[4] Wendt, F. 1933. Turbulente Strömungen zwischen zwei rotierenden konaxialen Zylindern, *Ing. Arch*. 4: 577-595.

[5] Bazilevs, Y. and I. Akkerman. 2010. Large eddy simulation of turbulent Taylor-Couette flow using isogeometric analysis and the residual-based variational multiscale method, *J. Comp. Phys.* 229: 3402-3414.

[6] Dong, S. 2008. Turbulent flow between counter-rotating concentric cylinders: a direct numerical simulation study, *J. Fluid Mech*. 615: 371–399.

[7] Kaye, J. and E.C. Elgar. 1958. Modes of adiabatic and diabatic fluid flow in an annulus with an inner rotating cylinder, *Trans. ASME: J. Heat Transfer* 80: 753–765.

[8] Nouri, J.M. and J.H. Whitelaw. 1994. Flow of Newtonian and non-Newtonian fluids in a concentric annulus with rotation of the inner cylinder. *Trans. ASME: J. Fluids Eng*. 116: 821–827.

[9] Nouri, J.M., and J.H. Whitelaw. 1997. Flow of Newtonian and non-Newtonian fluids in an eccentric annulus with rotation of the inner cylinder, *Int. J. Heat Fluid Flow* 18: 236–246.

[10] Naser, J.A. 1997. Prediction of newtonian and non-newtonian flow through concentric annulus with centerbody rotation. In: *International Conference on CFS in Mineral and Metal Processing and Power Generation*. CSIRO.

[11] Chung, S.Y. and H.J. Sung. 2005. Large-eddy simulation of turbulent flow in a concentric annulus with rotation of an inner cylinder, *Int. J. Heat and Fluid Flow* 26: 191–203.

[12] Kuosa, M., P. Sallinen and J. Larjola. 2004. Numerical and Experimental Modelling of Gas Flow and Heat Transfer in the Air Gap of an Electric Machine, *J. of Thermal Science* 13 (3): 264-278.

[13] Poncet S., S. Haddadi and S. Viazzo. 2011. Numerical modeling of fluid flow and heat transfer in a narrow Taylor–Couette–Poiseuille system, *Int. J. Heat and Fluid Flow* 32: 128–144.

[14] Elena, L. and R. Schiestel. 1996. Turbulence modeling of rotating confined flows. *Int. J. Heat Fluid Flow* 17: 283-289.

[15] Biage, M. and J.C.C. Campos. 2003. Visualization study and quantitative velocity measurements in turbulent Taylor-Couette flow tagging: a description of the transition to turbulence. *J. Braz. Soc. Mech. Sci. Eng.* 25 (4): 378-390.

[16] Abide, S. and S. Viazzo. 2005. A 2D compact fourth-order projection decomposition method, *J. Comp. Phys.* 206: 252-276.

[17] Beaubert, F. and S. Viazzo. 2003. Large Eddy Simulations of plane turbulent impinging jets at moderate Reynolds numbers, *Int. J. Heat Fluid Flow* 24 (4), 512–519.

[18] Viazzo, S., S. Poncet, E. Serre, A. Randriamampianina and P. Bontoux. 2011. High-order LES of confined rotor-stator flows. *Flow, Turbulence & Combustion,* to appear.

[19] Launder, B.E. and D.P. Tselepidakis. 1994. Application of a new second moment closure to turbulent channel flow rotating in orthogonal mode. *Int. J. Heat Fluid Flow* 15: 2-10.

[20] Poncet, S., R. Da Soghe and B. Facchini. 2010. RANS modelings of flows in rotating disk systems, In: *Eccomas CFD 2010*, Lisbon.

[21] OpenCFD. http://www.openfoam.com/.

[22] Weller, H.G., G. Tabor, H. Jasak and C. Fureby. 1998. A tensorial approach to computational continuum mechanics using object-oriented techniques. *Computers in Physics* 12 (6): 620-631.

[23] Menter, F.R. 1994. Two equation eddy viscosity turbulence model for engineering applications. *AIAA Journal* 32: 1598-1604.

[24] Yoshizawa, A. 1993. Bridging between eddy-viscosity-type and second-order models using a two-scale DIA. In: *9th Symposium on Turbulent Shear Flows* 3: 23.1.1-23.1.6. Kyoto, Japan.

[25] Menon, S., P.K. Yeung and W.W. Kim. 1994. Effect of subgrid models on the computed interscale energy transfer in isotropic turbulence. *AIAA paper* 94-2387.

[26] Menter, F.R. and Y. Egorov. 2005. A Scale-Adaptive Simulation Model using Two-Equation Models, *AIAA* paper 2005-1095, Reno/NV.

[27] Menter, F.R. and Y. Egorov. 2009. The scale-adaptive simulation method for unsteady flow predictions, Aerodynamic noise from wall-bounded flows, *Von Karman lecture series*, 03.

[28] STAR CCM+. http://www.cd-adapco.com/

[29] Smith, G.P. and A.A. Townsend. 1982. Turbulent Couette flow between concentric cylinders at large Taylor numbers, *J. Fluid Mech.* 123: 187-217.

[30] Tong, P., W.J. Goldburg, J.S. Huang and T.A. Witten. 1990. Anisotropy in turbulent drag reduction, *Phys. Rev. Lett.* 65: 2780-2783.

[31] Escudier, M.P., I.W. Gouldson and D.M. Jones. 1995. Flow of shear-thinning fluids in a concentric annulus. *Exp. Fluids* 18: 225-238.